

Provided for non-commercial research and education use.
Not for reproduction, distribution or commercial use.



This article appeared in a journal published by Elsevier. The attached copy is furnished to the author for internal non-commercial research and education use, including for instruction at the authors institution and sharing with colleagues.

Other uses, including reproduction and distribution, or selling or licensing copies, or posting to personal, institutional or third party websites are prohibited.

In most cases authors are permitted to post their version of the article (e.g. in Word or Tex form) to their personal website or institutional repository. Authors requiring further information regarding Elsevier's archiving and manuscript policies are encouraged to visit:

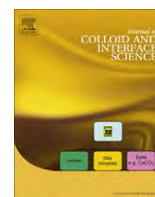
<http://www.elsevier.com/copyright>



Contents lists available at ScienceDirect

Journal of Colloid and Interface Science

www.elsevier.com/locate/jcis



Detergent–protein interactions in aqueous buffer suspensions of Photosystem I (PS I)

Dibyendu Mukherjee, Mark May, Bamin Khomami *

Sustainable Energy Education and Research Center (SEERC), University of Tennessee, Knoxville, TN 37996, USA
Department of Chemical and Biomolecular Engineering, University of Tennessee, Knoxville, TN 37996, USA

ARTICLE INFO

Article history:

Received 22 December 2010

Accepted 18 March 2011

Available online 9 April 2011

Keywords:

Photosystem I

Protein–protein interactions

Protein–detergent interactions

Aggregation

SAM

Jammed suspension

ABSTRACT

Systematic and uniform monolayer formation of Photosystem I (PS I) onto self-assembled monolayer (SAM) substrates to enable unidirectional electron transfer is crucial for its successful use in the fabrication of bio-hybrid solid-state electronic or photovoltaic devices. Yet, our recent studies (Mukherjee et al., 2010) indicate that surface self-assembly of PS I from aqueous buffer suspensions onto alkanethiolate SAM/Au substrates frequently leads to complex columnar structures due to solution phase protein aggregations. We investigate the effect of two prototypical non-ionic detergents, *n*-Dodecyl- β -D-Maltoside (DM) and Triton X-100 (TX-100), on protein–protein interactions via the protein–detergent interfacial chemistry. Dynamic light scattering (DLS) experiments are used to demonstrate the impact of relative protein/detergent concentrations on aggregation dynamics of PS I suspensions. In turn, the surface attachment characteristics of PS I adsorbed from the aforementioned suspensions onto SAM/Au substrate is examined by atomic force (AFM) microscopy. Our results indicate that relative concentration of PS I and detergents (DM or, TX-100) with respect to their critical micelle concentrations (CMC) determines the extent of self-association between PS I complexes driven by the screening induced by detergent micelles and/or, inter-protein distances. Such interfacial phenomena during the PS I–detergent complexation process drives the colloidal system through various regimes of phase separations, suspension and/or, de-aggregation, wherein individual PS I complexes can exist in a frustrated state that prevents favorable orientations for PS I–PS I interactions. The present study presents a novel strategy, heretofore not considered, for tailoring inter-protein distances and protein–protein interactions in solution phase, thereby allowing a superior control on the surface attachment of PS I onto SAM/Au substrates.

Published by Elsevier Inc.

1. Introduction

Colloidal studies of photosynthetic or light harvesting protein complexes such as Photosystems I and II (PS I and PS II), bacteriorhodopsin, LHC I and II, and *Rhodospirillum rubrum* offer specific structural and functional challenges since they are integral membrane proteins. Hence, a better understanding of the complex structure and functionality of these classes of proteins can enable their applications in biomimetic or, biomolecular devices or materials [1–4]. Specifically, the growing interest in photosynthetic membrane proteins as natural resources for photo-activated macromolecules has encouraged recent studies based on the concepts of colloidal science and soft matter physics to improve the utilization of these proteins in the aforementioned applications through their stabilization with various detergents [5]. Thus, while past research efforts have been directed towards tailoring

protein–detergent complexes to monitor the structural and functional activities of light harvesting chlorophyll a/b-protein complexes [6] or, crystallize photochemical reaction centers from *R. sphaeroides* [7,8], recent years have also seen similar efforts in characterizing the stability of bacteriorhodopsin [9] and LHC II [10]. To this end, detailed characterization of membrane protein interactions with non-ionic detergents typically used for their solubilization and stabilization in solution phase becomes critical in understanding the complexation processes involved in the replacement of phospholipids on the hydrophobic segments of membrane proteins by the hydrophobic moiety in the detergents [11,12] that closely mimic the native biological membrane of these proteins.

The aforementioned interest in the colloidal science of membrane protein suspensions has prompted studies aimed at developing a fundamental understanding of the solution phase aggregation of this class of proteins when stabilized with various anionic, cationic, zwitterionic or non-ionic detergents (or, surfactants). In particular, significant efforts have been focused on elucidating the complex interfacial chemistry in protein–detergent–lipid interactions that dictate the stability and mechanism of conformational

* Corresponding author at: Department of Chemical and Biomolecular Engineering, University of Tennessee, Knoxville, TN 37996, USA.

E-mail address: bkhomami@utk.edu (B. Khomami).

changes, or solution phase aggregations [13–18]. Specifically, detailed spectroscopic and/or scattering (both light and neutron) studies have been carried out to characterize the structural, interfacial and thermodynamic properties of two commonly found non-ionic amphiphilic detergents, Triton X-100 or TX-100 (octylphenol-polyethylene glycoether) [19–21] and DM (*n*-Dodecyl- β -D-Maltoside) [22–25] mainly due to their sensitivity and compatibility in isolating membrane proteins. While analytical centrifugation and sedimentation measurements in the past have revealed that the self-association behavior of myelin basic protein gets enhanced at low TX-100 concentrations [26], more recent protocols with gel filtration chromatography techniques have been specifically developed to analyze detergent binding and aggregation processes of membrane proteins using radiolabeled DM [27]. Moreover, small angle X-ray (SAXS) and neutron (SANS) scattering techniques have been extended to investigate the size and shape of pure DM micelles [28] as well as analyze and compare the structural organization of mixed membrane protein/detergent micelles in solution or in crystalline phase for both TX-100 and DM [29].

Our specific interest in the present study stems from the enormous potential of incorporating cyanobacterial PS I, that undergoes spontaneous charge separation to facilitate unidirectional electron transfer [30] upon exposure to light, into bio-hybrid solid-state electronic devices [1–3,31]. However, harnessing this potential requires development of robust techniques for the assembly of uniform and homogeneous films of photoactive PS I on suitable organic/inorganic substrates. In an effort to develop highly reproducible deposition strategies, one must address the frequently encountered problem in protein solutions, namely, solution phase aggregation. To this end, our recent studies have revealed that protein concentrations and driving forces play a significant role in altering the morphological assembly of PS I on SAM substrates when adsorbed from aqueous buffer solutions using gravity driven or electric field assisted directed deposition [4]. Commonly used self-assembly of PS I from buffer solutions onto hydroxyl-terminated alkanethiolate SAM/Au surfaces [3,32–35] and a few directed attachment of PS I to Au substrates using platinization techniques [36] have analyzed the attachment dynamics based on surface characterizations using microscopy (AFM) or spectroscopic techniques. Yet, our recent dynamic light scattering (DLS) data have demonstrated that the complex surface morphologies observed in most of these studies mainly arise due to protein–protein interactions in the solution phase [4]. Hence to develop robust techniques for deposition of PS I monolayer on various substrates, a much better understanding of the dynamics of colloidal suspension of PS I in prototypical non-ionic detergents such as TX-100 and DM is required.

Systematic characterization of the morphology and aggregation behavior of cyanobacterial PS I [37] or, the structural and conformational changes of PS I and PS II [38] when solubilized in TX-100 have provided useful insight into the thermostability and functional robustness of PS I and II outside their natural thylakoid membranes. Added to this, studies on membrane protein crystallization have begun to consider the role of critical micellar (CMC), solubilization (CSC) and aggregation (CAC) concentrations of various *n*-alkyl- β -D-Maltoside detergents in dictating the solubilization of trimetric PS I extracted from *Thermosynechococcus elongatus* (*T. elongatus*) [39]. Although such studies reveal the complexity of protein/detergent interaction studies, they fail to characterize the role of protein/detergent concentrations in tailoring the PS I–PS I interactions in colloidal phase in a way that they can be translated into a successful and uniform surface immobilization of PS I trimeric complexes. Such efforts, not being fully understood and implemented to date, are of great interest to the colloidal community working with biomolecules at interfaces.

To this end, the present study investigates the relative roles of non-ionic detergent molecules/micelles concentrations (i.e., CMC, CAC or CSC) and protein concentrations in tuning the solution phase protein aggregation behavior, thereby enabling a systematic control on the uniform monolayer of proteins adsorbed onto SAM/Au substrates from aqueous buffer solutions. Specifically in this study, we use the cyanobacterial PS I from *T. elongatus* as the integral membrane protein complex solubilized with two different non-ionic detergents, TX-100 and DM in 200 mM sodium phosphate buffer solution with pH = 7.0. Results are presented in terms of solution phase characterizations of PS I–detergent complex using DLS, along with specific AFM images to highlight the effect of PS I–detergent colloidal interactions on the surface topography of PS I complexes deposited from buffer solutions onto SAM/Au substrates.

2. Materials and methods

2.1. Chemicals and materials used

Commercial gold coated silicon wafers with titanium adhesion layer (Au thickness \sim 100 nm) were purchased from Platypus Technologies. Dibasic (Na_2HPO_4) and monobasic (NaH_2PO_4) sodium phosphate with >99% assay were purchased from Fisher Scientific to prepare the aqueous buffer solutions of 200 mM Na-Phosphate with pH = 7.0. Concentrated hydrochloric (HCl with \sim 38% assay) and nitric (HNO_3 with \sim 69.2% assay) acids purchased from Fisher Scientific were used to prepare fresh Aqua Regia. Ethanol (>99% purity) purchased from Decon Laboratory Inc. was used as the organic solvent to prepare thiol solutions and isopropanol (electronic grade with >99% purity) from Acros Organic was used as the organic cleaning reagent for all the substrates. Concentrated 11-mercapto-1-undecanol (5 mM in ethanol with 97% purity) was purchased from Sigma–Aldrich, *n*-Dodecyl- β -D-Maltoside (DM) was purchased from Gold Biotechnology whereas Triton X-100 (10% w/v aqueous solution) was obtained from Anatrace.

2.2. Methods and experimental set-up

2.2.1. Growth of *T. elongatus* and preparation of Photosystem I

The thermophilic cyanobacterium *T. elongatus* BP-1 was grown in 2L airlift fermenters (Bethesda Research Labs, Bethesda MD) in NTA media [40]. The details for the extraction and purification of the trimeric PS I complex from the grown *T. elongatus* cells are provided in our earlier work [4]. Based on spectrophotometer measured chlorophyll concentrations, the concentration of the extracted PS I trimers was estimated to be around $C_B = 1.42 \times 10^{-5}$ mol/L. PS I trimers were stored in aliquots of 1.5 mL at -80°C for future use.

2.2.2. Preparation of alkanethiolate SAM/Au substrates

Commercial Au coated Si wafers were freshly dipped in Aqua Regia (HNO_3 and HCl acids in volumetric ratio of 1:3 respectively). In turn, these freshly cleaved Au substrates (Au thickness \sim 60–70 nm) were immersed in 1 mM 11-mercapto-1-undecanol overnight (\sim 24–36 h) at room temperature in a chamber filled with inert dry N_2 . Thiolated Au substrates were washed in isopropanol, de-ionized water, and finally dried in dry N_2 stream. Monolayer formation was confirmed by measuring the thiol thickness on Au substrates at multiple spots using an ellipsometer. For the alkanethiol with C11 chain length used in this study, the thicknesses were measured to be around 0.9–1.1 nm.

Table 1
Physical properties of the detergents, DM and TX-100.

Chemical name	DM <i>n</i> -Dodecyl- β -D- Maltoside	TX-100 Octylphenolpoly (ethylene glycoether) _x
Molecular weight (g/mol)	510.6	650
Critical micelle concentration (CMC, mM)	0.18	0.24
Eqvt. hydrodynamic diameter (nm)	5.5–6.0	7.5–8.0

2.2.3. Preparation of colloidal suspension of PS I in buffer solutions

To investigate the effect the detergent concentrations on solution phase characteristics, colloidal solutions of PS I in 200 mM sodium phosphate buffer (pH = 7.0) were prepared with PS I concentrations of 7.2×10^{-5} mM in buffer solutions stabilized with different concentrations of the non-ionic detergents, DM and TX-100 with respect to their respective CMC values of 0.18 (CMC_{DM}) and 0.24 (CMC_{TX}) mM respectively. Detailed technical specifications regarding the physical properties of DM and TX-100 are provided in Table 1.

Specifically, for the studies focused on the role of DM in controlling the PS I structures in solution, solution phase characterizations were carried out for varying concentrations of PS I suspensions in buffer solutions stabilized with fixed DM concentrations of: (1) 0.02% w/v (~ 0.4 mM, i.e., $2.2\text{CMC}_{\text{DM}}$) and (2) 0.002% w/v (~ 0.04 mM i.e., $0.2\text{CMC}_{\text{DM}}$) in different PS I concentrations as discussed later in details in Section 3. PS I concentrations ranging between $C_{\text{PSI}} = 9.1 \times 10^{-6}$ mM (1600 \times dilution) – 5.4×10^{-4} mM (25 \times dilution) were chosen for sample preparations. The dilutions indicated within bracket next to the C_{PSI} values, as shall be reported in the rest of this article, are with respect to the base concentrations of $C_{\text{B}} = 1.42 \times 10^{-5}$ mol/L for the extracted and purified PS I samples as reported earlier.

2.2.4. Preparation of PS I/SAM/Au substrates

Surface immobilization of PS I used the solution phase self-assembly techniques [4] of immersing the alkanethiolate SAM/Au substrates for 5 min. in different PS I concentrations (9.1×10^{-6} mM to 5.4×10^{-4} mM) prepared with 200 mM Na-Phosphate aqueous buffer solutions (pH = 7.0) and specifically stabilized with DM concentrations of 0.02% w/v (i.e., $2.2\text{CMC}_{\text{DM}}$) to demonstrate the effectiveness of DM in controlling PS I–PS I interactions (discussed in Section 3).

2.2.5. Atomic Force Microscopy (AFM)

All surface topography images were collected on an Asylum Research Inc. make Atomic Force Microscopy (AFM) instrument (Model: MFP-3D-BIO) in the tapping mode. All topographical images were recorded using a Silicon tip compatible with softer biological materials (Make: Olympus; Model: AC240TS) having a force constant of 2 N/m and a resonant frequency of 70 kHz.

2.2.6. Dynamic light scattering (DLS)

Dynamic light scattering data used to analyze PS I aggregation and individual sizes were collected using a Malvern Instruments make Zetasizer operating with a laser of 632.8 nm wavelength. All size distributions obtained from DLS data were collected using a 178 $^\circ$ backward scattering and averaged over six experimental runs each of which were summed up over 12–13 time correlograms fitted by the in-built software of the Zetasizer. All sizes reported in the size distribution data are the equivalent spherical hydrodynamic radius as estimated from Stokes–Einstein relation wherein the effective thermo physical properties of 200 mM Na-

Phosphate aqueous buffer solutions with pH = 7.0 were taken into consideration.

3. Results and discussion

3.1. Different detergent concentrations at fixed PS I concentrations

The particle size distributions (PSD in terms of volume distribution, %) from DLS measurements on solution samples with fixed PS I concentration of $C_{\text{PSI}} = 7.2 \times 10^{-5}$ mM (Figs. 1A–C and D–F) demonstrate the aggregation behaviors of PS I complexes, when stabilized with TX-100 and DM respectively, for different detergent concentrations (indicated by $C/\text{CMC}|_{\text{TX}}$ and $C/\text{CMC}|_{\text{DM}}$ values in Fig. 1). In conjunction to the PSD, the corresponding normalized volume averaged hydrodynamic diameters ($D_{\text{Hyd}}/D_{\text{PSI}}$) plotted against detergent concentrations normalized by their respective CMC values ($C_{\text{Detergent}}/\text{CMC}$) is shown in Fig. 2. These two figures clearly demonstrate the evolution of mean cluster sizes due to PS I aggregation in relation to the respective CSC and CDC values for TX-100 and DM. It is noted that D_{Hyd} is estimated from respective PSDs in Fig. 1 and the equivalent hydrodynamic diameter of single PS I trimer, $D_{\text{PSI}} \sim 21$ nm is estimated based on its shape factor, i.e., an oblate spheroid [41] with dimensions: 30 nm diameter \times 9 nm height (refer to Fig. 4; details provided in our earlier work [4]).

The large aggregation observed for $C/\text{CMC}|_{\text{TX}} = 0.5$ ($<\text{CMC}_{\text{TX}}$) and 1.0 ($\sim\text{CMC}_{\text{TX}}$) in Fig. 1A, is related to the inability of the detergents to solubilize the proteins. This phenomenon persists as TX-100 concentration is increased to $C/\text{CMC}|_{\text{TX}} = 1.5$, as indicated by $D_{\text{Hyd}}/D_{\text{PSI}} \sim 70$ –90 for the respective $C/\text{CMC}|_{\text{TX}}$ cases in Fig. 2 (gray dotted line on x-axis indicates the respective $C_{\text{Detergent}} = \text{CMC}$ for TX-100 or DM). Visual inspection of the respective solution samples in each of these cases indicate heavy precipitation, and hence phase separation, of the PS I complexes thereby supporting our earlier observation (typical inset photographs representing each of the cases in Fig. 1A). As the detergent concentration is increased to $C/\text{CMC}|_{\text{TX}} = 1.8$, the PSD (Fig 1B) indicates a disintegration of the large peaks centered on the size bins ≥ 1000 nm into sizes widely distributed across 100–1000 nm ranges. As expected, in conjunction with this shift, a marked drop in mean cluster sizes ($D_{\text{Hyd}}/D_{\text{PSI}} \sim 3$ in Fig. 2) is also observed. It should be pointed out that visual inspection of all the samples beyond $C/\text{CMC}|_{\text{TX}} = 1.8$ indicated complete solubilization of the PS I complexes in the buffer solutions even after weeks of incubation (typical inset photographs, each set of which represents the respective cases in Fig. 1B and C). Thus, $C/\text{CMC}|_{\text{TX}} = 1.8$ marks the onset of solubilization (i.e., $\text{CSC}_{\text{TX}} \gg \text{CMC}_{\text{TX}}$ as marked in Fig. 2), wherein TX-100 detergent molecules, in addition to undergoing attachment with PS I, physically screen the protein clusters from each other that allows the suspension of aggregated PS I clusters in the buffer solutions. A further increase in TX-100 concentration ($C/\text{CMC}|_{\text{TX}} = 2.0$) results in a complete shift of the PSD to a single uniform peak at ~ 18 –20 nm that corresponds to the equivalent hydrodynamic diameter of a single PS I trimeric complex ($D_{\text{PSI}} \sim 21$ nm) and is corroborated by $D_{\text{Hyd}}/D_{\text{PSI}} \sim 1.0$ in Fig. 2 (gray dotted line on y-axis indicates $D_{\text{Hyd}} = D_{\text{PSI}}$). Thus, $C/\text{CMC}|_{\text{TX}} = 2.0$ marks the onset of de-aggregation of PS I clusters into individual trimeric complexes (i.e., $\text{CDC}_{\text{TX}} \gg \text{CMC}_{\text{TX}}$ as marked in Fig. 2) wherein TX-100 molecules, in excess of the ones associated with the PS I, form spherical micelles that physically screen the PS I trimers from each other. This impedes the favorable top–bottom PS I–PS I associations due to the favorable electrostatic interactions arising due to the inherent dipole moment [42] of the PS I complexes that otherwise lead to the columnar structures [4]. Higher detergent concentrations ($C/\text{CMC}|_{\text{TX}} \sim 2.6$ –5.1) result in PSDs (Fig. 1C) that exhibit large scatter over a wide range of size domains ranging from <1 nm (less

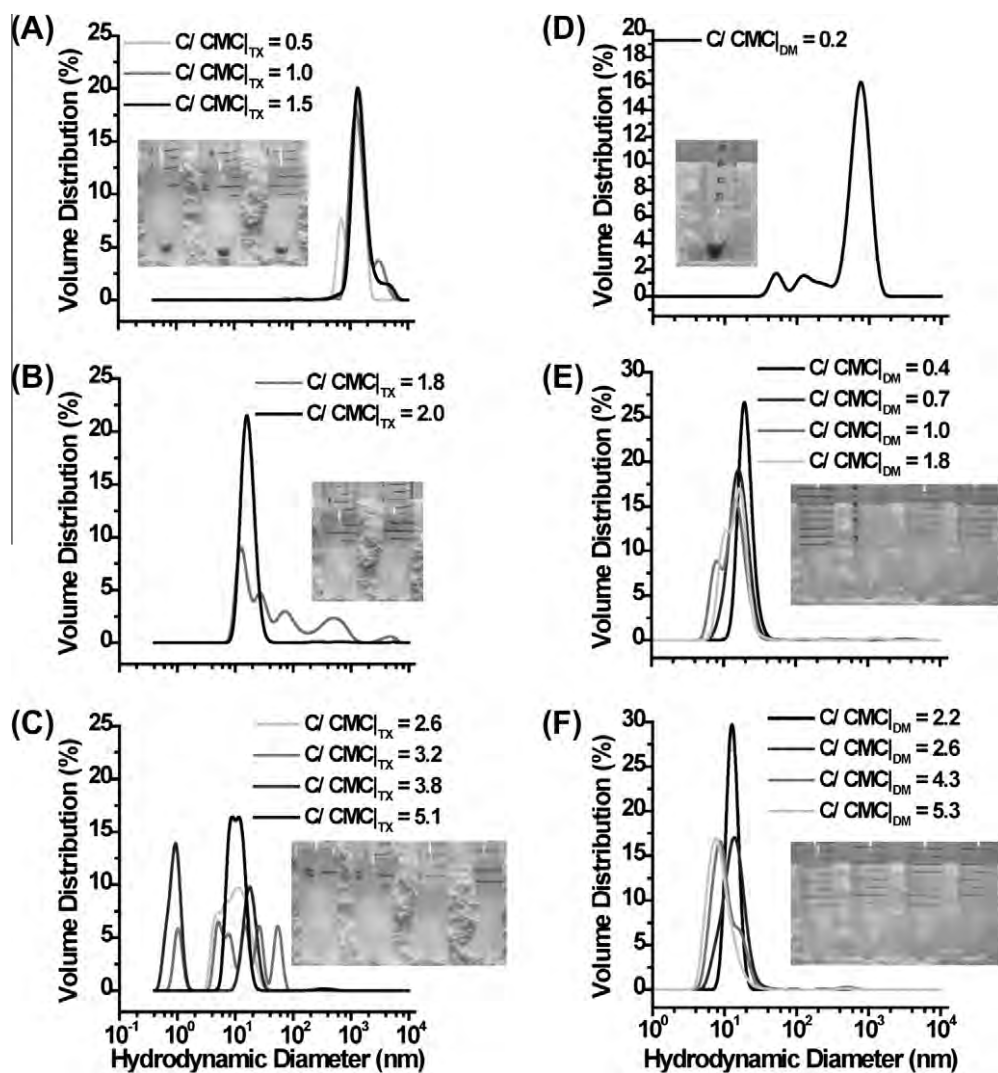


Fig. 1. Particle size distributions (PSD in volume distribution, %) as obtained from dynamic light scattering (DLS) measurements on solution samples with fixed PS I concentration of $C_{PSI} = 7.2 \times 10^{-5}$ mM in 200 mM sodium phosphate buffer (pH = 7.0) stabilized with varying detergent concentrations of: (A–C) C/CMC_{TX} for TX-100 and (D–F) C/CMC_{DM} for DM. (Insets: Sample photographs of PS I solutions representing each of the detergent concentration ranges where PS I complexes precipitate or, solubilize).

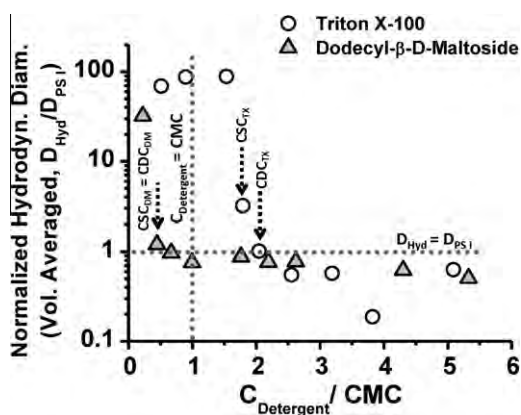


Fig. 2. Variation of volume averaged hydrodynamic diameters estimated from the respective PSDs in Fig. 1 and normalized by the equivalent hydrodynamic diameter of a single PS I trimer ($D_{PSI} \sim 21$ nm), i.e., D_{Hyd}/D_{PSI} as a function of different detergent concentrations normalized by their respective CMC values, i.e., $C_{Detergent}/CMC$.

than TX-100 micelle diameter ~ 6 – 7 nm) up to >100 nm ($>D_{PSI} \sim 21$ nm). This can be attributed to the possible disintegra-

tion or denaturation of the membrane protein into smaller fragments of varying sizes, a phenomenon reported in an earlier work for higher detergent concentrations of TX-100 [38].

In contrast, for PS I solutions stabilized with DM, the peak size at ~ 1000 nm only appear at $C/CMC_{DM} = 0.2$ (Fig. 1D) that corresponds to $D_{Hyd}/D_{PSI} \sim 32$ as shown in Fig. 2. As the DM concentration is increased to $C/CMC_{DM} = 0.4$ and 0.7 (Fig. 1E), the PSD peak distinctly shifts to the much smaller size bins ~ 18 – 20 nm (closer to the estimated $D_{PSI} \sim 21$ nm) with a corresponding $D_{Hyd}/D_{PSI} \sim 1.0$ (Fig. 2). It should be noted that, except for $C/CMC_{DM} = 0.2$ (typical inset photograph is representative of the particular case in Fig. 1D), visual inspection of the solution samples with $C/CMC_{DM} \geq 0.4$ did not exhibit any precipitation (typical inset photographs represent each of the respective cases in Fig. 1E and F). Hence, it is concluded that for PS I samples stabilized with DM, $C/CMC_{DM} = 0.4$ marks the simultaneous onset of solubilization ($CSC_{DM} = CDC_{DM}$) and de-aggregation (CDC_{DM}) as marked by $CSC_{DM} = CDC_{DM}$ in Fig. 2. Any further increase in DM concentration up to $C/CMC_{DM} = 1.8$ results in a continuous incremental shift in the PSD to lower sized bins. Finally, with higher detergent concentrations ($C/CMC_{DM} = 2.2$ – 5.3 in Fig. 1F) the PSDs continue to exhibit a steady decrease in the peak sizes to ~ 15 – 17 nm for

$C/CMC_{DM} = 2.2$ and 2.8 . Specifically, for $C/CMC_{DM} = 4.3$, the weakening of the peak at ~ 20 nm concurs with a corresponding enhancement of the peak at ~ 9 – 10 nm, which eventually shifts to a single uniform peak centered on ~ 6 – 7 nm for the $C/CMC_{DM} = 5.3$. The emergence of the small secondary peaks at ~ 6 – 7 nm for $C/CMC_{DM} = 1.0$ and 1.8 (Fig. 1E) along with the steady shift in PSD to a more pronounced peak at ~ 7 nm for $C/CMC_{DM} = 2.2$ – 5.3 (Fig. 1F) is attributed to the larger volume fraction of spherical DM micelles whose sizes are typically of the order ~ 6 nm (refer to Table 1). But, as seen from Fig. 2, due to the attainment of CSC_{DM} or CDC_{DM} values at $C_{Detergent}/CMC \ll 1$, the PS I complexes retain their individual trimetric form ($D_{Hyd}/D_{PSI} \sim 1.0$) in the colloidal suspension over a wide range of DM concentrations ($C_{Detergent}/CMC \sim 0.4$ – 2.2). This is further corroborated by the uniform and steady peak sizes centered on ~ 18 – 20 nm (corresponding to $D_{PSI} \sim 21$ nm) in Figs. 1E and F for $C/CMC_{DM} = 0.4$ ($\ll CMC_{DM}$) to 2.2 ($> CMC_{DM}$).

These observations clearly suggest that DM, when compared to TX-100, is a more effective and stable detergent for PS I colloidal systems due to its higher affinity for PS I lipid membranes that promotes an energetically favored PS I-DM interactions even at DM concentrations $< CMC_{DM}$. The aforementioned results turn the focus of the present study in the subsequent section towards the roles of relative concentrations of PS I and DM in driving the colloidal chemistry needed to tune surfactant mediated PS I-PS I interactions in aqueous buffer solutions of PS I.

3.2. Different PS I concentrations at fixed DM concentrations

PSDs from DLS measurements on solution samples with different PS I concentrations (9.1×10^{-6} mM (1600 \times dilution) to 5.4×10^{-4} mM (25 \times dilution)), when stabilized with a fixed low DM concentration of $C/CMC_{DM} = 0.2$ ($\ll CMC_{DM}$, i.e., the first case reported in Fig. 1D), are shown in Fig. 3A–C. Large scale PS I aggregation is indicated by the wide scatter in the PSD (50 nm to >1000 nm in Fig. 3A) for $C_{PSI} = 9.1 \times 10^{-6}$ mM (1600 \times) and 1.8×10^{-5} mM (800 \times) that becomes aggravated when PS I concentration is increased to 3.6×10^{-5} mM (400 \times) as indicated by the peak shifts to larger sized bins. Eventually, at higher PS I concentrations ($C_{PSI} = 7.2 \times 10^{-5}$ mM (200 \times) to 1.4×10^{-4} mM (100 \times)), bulk aggregations due to enhanced PS I-PS I interactions [4] result in a complete shift of the size distributions to uniform peaks >1000 nm (Fig. 3B). But, any further increase in C_{PSI} up to $\sim 2.8 \times 10^{-4}$ mM (50 \times) shows a unique behavior wherein, instead of a higher degree of agglomeration, the peak size shifts from >1000 nm (Fig. 3B) to ~ 45 – 50 nm (Fig. 3C). The same trend continues as PS I concentration is further increased to $C_{PSI} = 5.4 \times 10^{-4}$ mM (25 \times) in Fig. 3C, wherein the size distribution eventually equilibrates with the peak size around ~ 20 – 22 nm, in agreement with the equivalent hydrodynamic diameter of single PS I trimer ($D_{PSI} \sim 21$ nm). This phenomenon is indicative of the emergence of a high number density of closely packed PS I trimeric complexes in the solution samples wherein the inter particle distances (represented as $R_{PSI-PSI}$ in the schematic inset in Fig. 4) are on the order of the length scales that prevent rotational diffusions (discussed in details later). Such a situation thwarts the preferential alignments required for protein aggregation, thereby leaving the individual PS I complexes in a frustrated state leading to a jammed suspension.

To further investigate this phenomenon, normalized hydrodynamic diameters, D_{Hyd}/D_{PSI} (left y-axis in Fig. 4) as a measure of PS I cluster sizes, is plotted in conjunction with the average inter-protein distances in solution ($R_{PSI-PSI}$ in nm; right y-axis in Fig. 4) as a function of varying PS I concentrations. It should be noted that the average $R_{PSI-PSI}$ values in nm (indicated by the schematic inset in Fig. 4) are estimated, based on the assumption of uniform PS I distribution, from the volume fraction of PS I com-

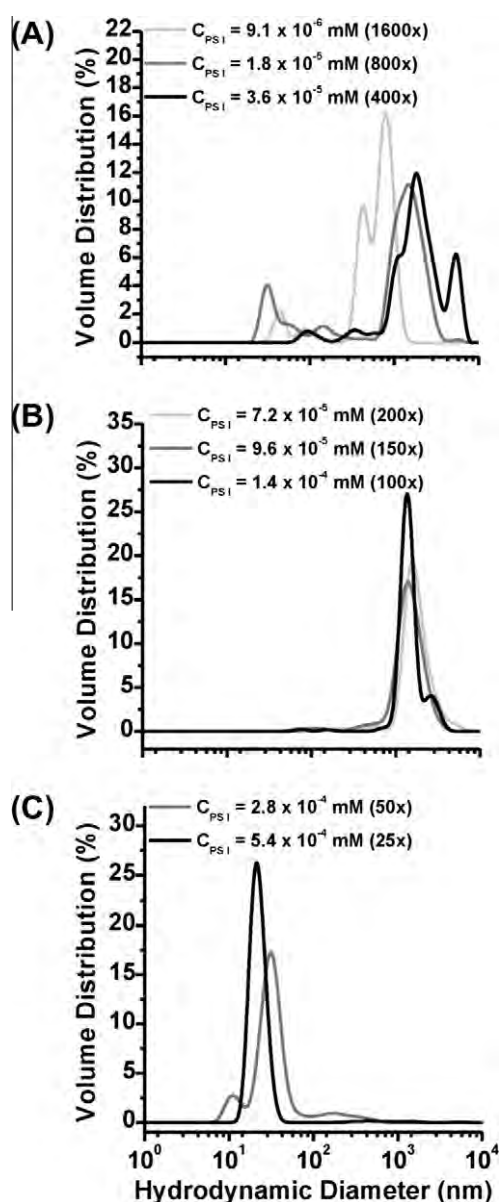


Fig. 3. (A–C) Particle size distributions (PSD in volume distribution, %) as obtained from dynamic light scattering (DLS) measurements on PS I solution samples with $C_{PSI} = 9.1 \times 10^{-6}$ mM (1600 \times dilution) to 5.4×10^{-4} mM (25 \times dilution) in 200 mM sodium phosphate buffer (pH = 7.0) stabilized with a fixed low DM concentration of $C/CMC_{DM} = 0.2$ (~ 0.04 mM DM $\ll CMC_{DM}$).

plexes suspended in the solution phase prior to the onset of agglomeration and the volume of a single PS I-detergent complex (taking into account the detergent ring around the lipid membrane belt of the PS I complex as shown in the inset in Fig. 4). With the DM concentration fixed at $C/CMC_{DM} = 0.2$ ($C_{DM} \ll CMC_{DM}$), the inter-protein distances $R_{PSI-PSI}$ in Fig. 4 exhibit a power law decay with increasing PS I concentrations. In relation to this, aggregated clusters ($D_{Hyd}/D_{PSI} \sim 30$ – 40) are formed at lower PS I concentrations ($C_{PSI} = 9.1 \times 10^{-6}$ mM (1600 \times) and 1.8×10^{-5} mM (800 \times)) where $R_{PSI-PSI} \sim 270$ – 350 nm. But with increasing C_{PSI} , the cluster sizes increase at $C_{PSI} = 3.6 \times 10^{-5}$ mM (400 \times), and approach a plateau region around $D_{Hyd}/D_{PSI} \sim 96$ – 100 up to $C_{PSI} = 9.6 \times 10^{-5}$ mM (150 \times), thereby indicating heightened PS I-PS I interactions when $R_{PSI-PSI}$ ranges ~ 130 – 210 nm.

Beyond this point, a slow decrease in the cluster sizes ($D_{Hyd}/D_{PSI} \sim 78$ – 80) is observed as PS I concentration is increased to

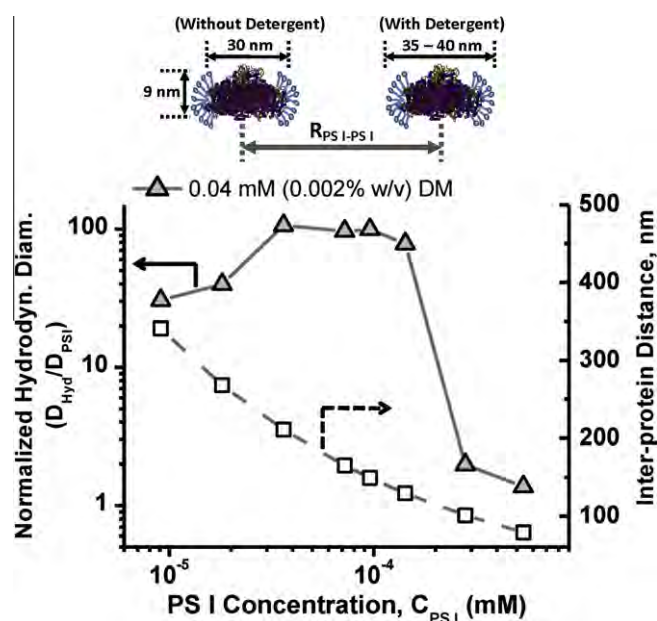


Fig. 4. Variation of normalized volume averaged hydrodynamic diameters, D_{Hyd}/D_{PSI} (left y-axis) as estimated from the respective PSDs in Fig. 3 and the average inter-protein distances in solution, $R_{PSI-PSI}$ (nm, right y-axis) as a function of varying PS I concentrations, C_{PSI} (mM). (Inset: Schematic showing the mean inter-protein distance, $R_{PSI-PSI}$ (nm) as estimated from the volume fraction of PS I complexes and the mean diameter of a single PS I trimeric complex on taking into account the detergent molecules attached to the rim of the lipid membrane belt of the PS I complex).

$C_{PSI} = 1.4 \times 10^{-4}$ mM (100 \times), thereby indicating that the aggregation process is hindered. Finally, at higher concentrations of $C_{PSI} = 2.8 \times 10^{-4}$ mM (50 \times) and 5.4×10^{-4} mM (25 \times), a marked drop in the cluster sizes to almost that of single trimers is observed ($D_{Hyd}/D_{PSI} \sim 2$ and 1.3 and a rapid drop in the respective $R_{PSI-PSI}$ values to 100 and 79 nm respectively in Fig. 4). It should be noted that the aforementioned phenomenon indicates bulk aggregation at $R_{PSI-PSI} > 300$ nm and an attractive potential that enhances the aggregation processes between $R_{PSI-PSI} \sim 130$ –210 nm, both of which are commonly observed in most protein solution systems [43,44]. But the rapid reduction in cluster sizes at $R_{PSI-PSI} < 100$ nm is indicative of a jammed suspension wherein PS I trimers find themselves in a frustrated state that thwarts structural arrangements favorable for aggregation. Specifically, one can approximate that the major diameter of the oblate spheroid shaped PS I being ~ 40 nm (inset in Fig. 4), an inter-protein distance of $R_{PSI-PSI} \sim 80$ –100 nm could easily hinder any rotational movements of PS I.

Furthermore, PSDs in Figs. 5A–C illustrate the PS I aggregation behavior in buffer suspensions with different PS I concentrations ($C_{PSI} = 9.1 \times 10^{-6}$ mM to 2.8×10^{-4} mM) and a fixed high DM concentration of $C/CMC_{DM} = 2.2$ ($\gg CMC_{DM}$). PSD for the lowest PS I concentration ($C_{PSI} = 9.1 \times 10^{-6}$ mM (1600 \times)), being largely volume weighted by the DM micelles, indicates a single peak at ~ 6 –7 nm (Fig. 5A) which coincides with the control peak size (represented with a dotted line) for DM micelles ($D_{Micelles} \sim 6$ nm as mentioned in Table 1; marked by the “dotted” arrow). The control data was obtained from the PSD collected for blank buffer treated with DM ($C/CMC_{DM} = 2.2$) but devoid of any PS I. Upon increasing PS I concentration to $C_{PSI} = 1.8 \times 10^{-5}$ mM (800 \times), the emergence of the peak at ~ 20 nm (commensurate with $D_{PSI} \sim 21$ nm; the “long dash” arrow) in Fig. 5A can be rationalized by the increase in the relative volume fractions of PS I trimers, while the decrease in the peak size at ~ 7 nm ($\sim D_{Micelles}$) and the surge of the two secondary peaks at ~ 2 –4 nm ($< D_{Micelles}$; the “dash-dot” arrow)

suggest a simultaneous decrease in the number density of DM micelles along with the creation of smaller sized DM clusters due to the possible fragmentation of the micelles. This process is continued further for $C_{PSI} = 3.6 \times 10^{-5}$ mM (400 \times) and 7.2×10^{-5} mM (200 \times) until the major peak size increasingly shifts through intermediate size ranges of ~ 12 –17 nm along with the PSD broadening towards the 20 nm size bin ($\sim D_{PSI}$; see Fig. 5B). In conjunction with this, the micellar peak size ($\sim D_{Micelles}$; the “dotted” arrow) shows a rapid decay along with a simultaneous enhancement of the smaller peak size ($< D_{Micelles}$; the “dash-dot” arrow). Finally, while the PSDs in Fig. 5C distinctly indicate a shift in the major peaks to ~ 20 nm ($\sim D_{PSI}$; the “long dash” arrow) for both $C_{PSI} = 1.4 \times 10^{-4}$ mM (100 \times) and 2.8×10^{-4} mM (50 \times), the strong secondary peak at ~ 4 –5 nm ($< D_{Micelles}$; the “dash-dot” arrow) for $C_{PSI} = 1.4 \times 10^{-4}$ mM (100 \times) eventually disappears for the $C_{PSI} = 2.8 \times 10^{-4}$ mM (50 \times) case. Also, it is noted that the micellar peak ($\sim D_{Micelles}$; the dotted arrow) ceases to exist for both $C_{PSI} = 1.4 \times 10^{-4}$ mM (100 \times) and 2.8×10^{-4} mM (50 \times).

The aforementioned processes create an overall picture of a dynamically evolving system in which the strong affinity of DM molecules for the lipid membranes on PS I complexes results in an energetically favored PS I-DM interactions over DM-DM interactions in solution phase. To this end, an increasing PS I number density in the buffer solutions promote fragmentation of DM molecules from micelles (the continuous decrease in peak size at $D_{Micelles} \sim 7$ nm along with the simultaneous increase in smaller peak sizes ~ 2 –4 nm in Figs. 5A–C) that preferentially attach to the PS I trimers to generate a higher volume fraction of PS I-DM complexes (the surge in the peak size around $D_{PSI} \sim 21$ nm in Fig. 5C). Furthermore, when stabilized by a high DM concentration $\gg CMC_{DM}$ ($C/CMC_{DM} = 2.2$), the solutions with a wide range of PS I concentrations ($C_{PSI} = 9.1 \times 10^{-6}$ mM to 2.8×10^{-4} mM) never showed any aggregation as evident from Figs. 5. A–C indicating no cluster sizes > 20 –30 nm. This implies that the number density of DM micelles being much greater than that for PS I trimers (~ 1500 –2000 even for the highest PS I concentration of $C_{PSI} = 2.8 \times 10^{-4}$ mM), the PS I complexes are physically screened from each other. Such observations also support our earlier explanation of jammed suspensions where the PS I trimers co-exist in a frustrated state that prevents favorable orientations for aggregation. Attainment of such jammed states can bear serious implications in terms of controlling the inter-protein distances in the solution phase itself, thereby allowing superior control over driving individual PS I trimers onto chemically tailored SAM/Au substrates to create uniform and homogeneous PS I monolayer devoid of any PS I-PS I interactions.

AFM images in Fig. 5D–F for PS I trimers attached via gravity-driven adsorption process from buffer solutions stabilized by DM where $C/CMC_{DM} = 2.2$ further corroborate our observations. The surface topographies, as attained for depositions from buffer solutions with high PS I concentrations of $C_{PSI} = 1.4 \times 10^{-4}$ mM (100 \times), 2.8×10^{-4} mM (50 \times) and 1.4×10^{-3} mM (10 \times dilution, i.e. at extremely high PS I concentrations), are devoid of any PS I aggregates. In contrast to the highly aggregated columnar structures seen in our earlier deposition studies of PS I on SAM/Au substrates from buffer solutions with TX-100 as the detergent [4], the morphological arrangements in Fig. 5D–F are very uniform. Thus, the population density of PS I trimers (number of PS I/unit area) on the substrate increases from very sparse distribution for $C_{PSI} = 1.4 \times 10^{-4}$ mM (100 \times) to a uniform, dense and homogeneous distribution devoid of any aggregated structures even at very high concentration cases of $C_{PSI} = 1.4 \times 10^{-3}$ mM (10 \times), thereby allowing systematic monolayer formation. These results point towards a highly effective method of tailoring the morphology of PS I/SAM/Au substrates by monitoring the detergent mediated protein-protein interactions in the solution phase.

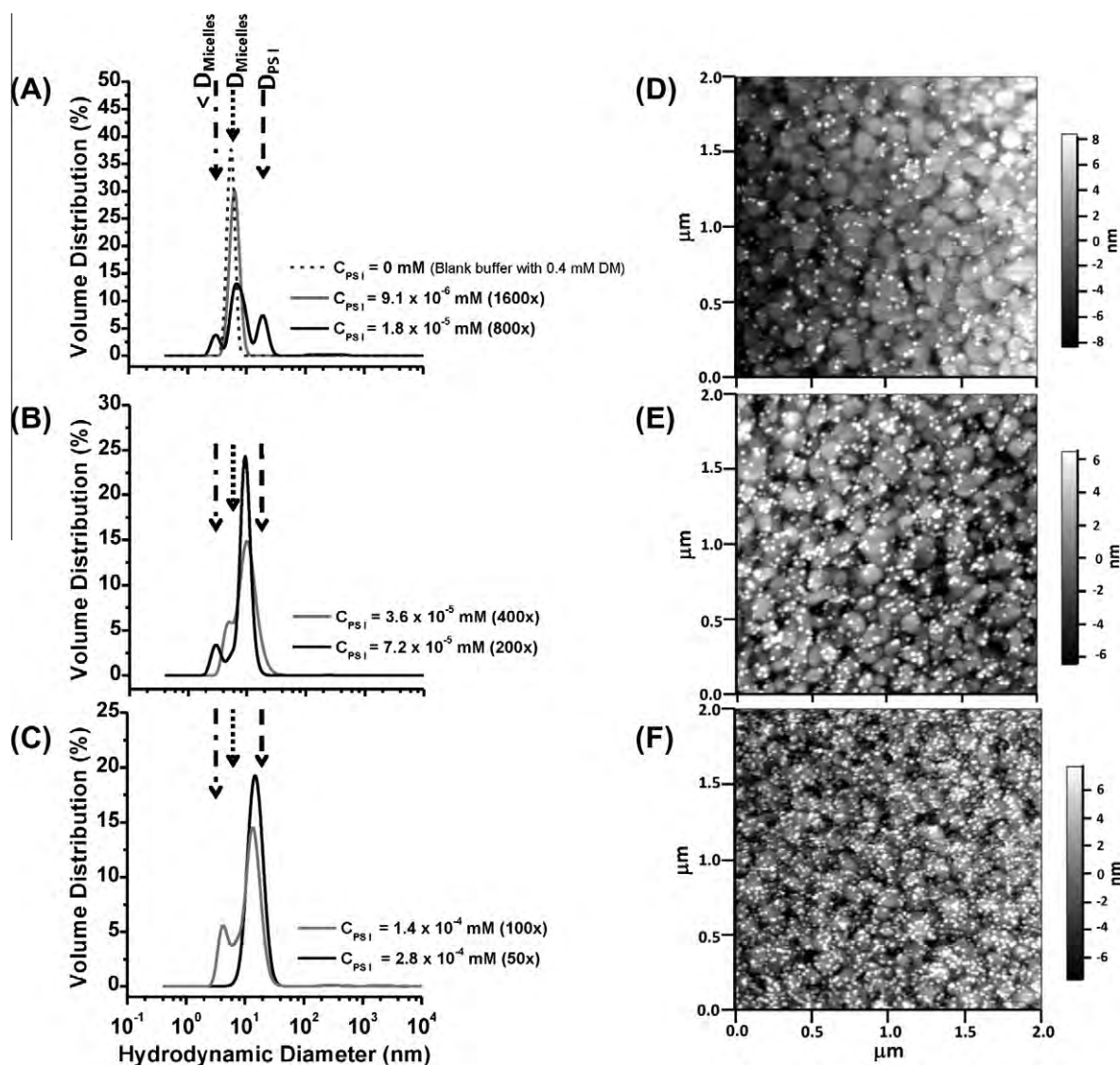


Fig. 5. (A–C) Particle size distributions obtained from DLS measurements on PS I solution samples with $C_{\text{PSI}} = 9.1 \times 10^{-6}$ mM (1600 \times dilution) to 2.8×10^{-4} mM (50 \times dilution) in 200 mM sodium phosphate buffer (pH = 7.0) stabilized with a fixed high DM concentration of $C/\text{CMC}_{\text{DM}} = 2.2$ (~ 0.4 mM DM \gg CMC_{DM}). $C_{\text{PSI}} = 0$ mM represents the control PSD collected for blank buffer treated with 0.4 mM DM; (D–F) AFM images of the surface topographies of depositions onto SAM/Au substrates from buffer solutions with high PS I concentrations of $C_{\text{PSI}} =$ (D) 1.4×10^{-4} mM (100 \times dilution), (E) 2.8×10^{-4} mM (50 \times dilution) and (F) 1.4×10^{-3} mM (10 \times dilution) stabilized with 0.4 mM DM ($C/\text{CMC}_{\text{DM}} = 2.2$).

4. Conclusion

Our findings demonstrate that detergents (or, surfactants) (TX-100 and DM in this study) play an intricate role in tuning PS I–PS I interactions through PSI-detergent colloidal chemistry, thereby dictating the solution phase aggregation of PS I leading to complex protein morphologies. The onset of PS I solubilization and de-aggregation in buffer solutions stabilized with low DM concentrations ($C/\text{CMC}_{\text{DM}} \ll 1$) facilitates the existence of individual PS I trimers over a wide range of DM concentrations, thereby suggesting that DM, as compared to TX-100, is a more robust and stable detergent that allows better control over solution-phase PS I–PS I interactions. Furthermore, buffer solutions with low PS I concentrations ($C_{\text{PSI}} = 1.8 \times 10^{-5}$ mM) and large inter-protein distances ($R_{\text{PSI-PSI}} > 300$ nm), when stabilized with low DM concentrations ($C/\text{CMC}_{\text{DM}} \leq 0.4$), give rise to bulk aggregation that gets enhanced for $C_{\text{PSI}} = 3.6 \times 10^{-5}$ mM to 1.4×10^{-4} mM where $R_{\text{PSI-PSI}} \sim 100$ –300 nm, thereby indicating an attractive PS I–PS I interactions.

For higher PS I concentrations ($C_{\text{PSI}} \geq 2.8 \times 10^{-4}$ mM), where $R_{\text{PSI-PSI}} \sim 80$ –100 nm, the close proximity of PS I trimers (major diameter of PS I ~ 40 nm) can effectively inhibit rotational diffusions and hence, prevent favorable orientations driven by the inherent PS I dipole moment that facilitates the top–bottom PS I–PS I associations. In such a situation, the PS I trimers are left in a frustrated state that results in jammed suspensions. On the other hand, PS I buffer solutions stabilized with high DM concentrations ($C/\text{CMC}_{\text{DM}} \geq 2.2$) does not indicate any bulk aggregation for a wide range of PS I concentrations, which can be attributed to a large volume fraction of DM micelles physically screening the PS I trimers from interacting with each other. Thus, relative concentrations of detergent micelles and PS I complexes can induce specific steric hindrances driven by the inter-protein distances, that finally determines the nature of PS I–PS I interactions in solution phase. The attainment of the aforementioned jammed suspensions allow a systematic and uniform distribution of the individual PS I trimeric complexes in the solution phase which, when driven to

SAM/Au substrates, are able to create uniform and homogenous surface morphology devoid of PS I–PS I lateral interactions. Such high-level of control on the surface morphology of PSI/SAM/Au substrates attained by tuning the surfactant mediated solution phase interfacial chemistry can be very promising for future work on synthesis of advanced bio-interfaces for bio-hybrid photovoltaic/electronic devices or sensors.

Acknowledgments

This work was funded by Sustainable Energy Education and Research Center (SEERC) at UTK. Partial support for DM was provided by the Gibson Family Fellowship.

References

- [1] R. Das, P.J. Kiley, M. Segal, J. Norville, A.A. Yu, L.Y. Wang, S.A. Trammell, L.E. Reddick, R. Kumar, F. Stellacci, N. Lebedev, J. Schnur, B.D. Bruce, S.G. Zhang, M. Baldo, *Nano Lett.* 4 (2004) 1079.
- [2] L. Frolov, Y. Rosenwaks, C. Carmeli, I. Carmeli, *Adv. Mater.* 17 (2005) 2434.
- [3] I. Carmeli, L. Frolov, C. Carmeli, S. Richter, *J. Am. Chem. Soc.* 129 (2007) 12352.
- [4] D. Mukherjee, M. May, M. Vaughn, B.D. Bruce, B. Khomami, *Langmuir* 26 (2010) 16048.
- [5] G. Palazzo, *Curr. Opin. Colloid Interface Sci.* 11 (2006) 65.
- [6] P.J.G. Butler, W. Kuhlbrandt, *Proc. Natl. Acad. Sci. USA* 85 (1988) 3797.
- [7] M. Roth, B. Arnoux, A. Ducruix, F. Reisschusson, *Biochemistry* 30 (1991) 9403.
- [8] P.A. Marone, P. Thiyagarajan, A.M. Wagner, D.M. Tiede, *J. Cryst. Growth* 207 (1999) 214.
- [9] M.G. Santonicola, A.M. Lenhoff, E.W. Kaler, *Biophys. J.* 94 (2008) 3647.
- [10] M.B. Cardoso, D. Smolensky, W.T. Heller, H. O'Neill, *J. Phys. Chem. B* 113 (2009) 16377.
- [11] S. Khamlichy, M.J. Loirat, D. Blanchard, M. Lemaire, P. Bailly, J.P. Cartron, O. Bertrand, *J. Biochem. Biophys. Methods* 29 (1994) 123.
- [12] M. le Maire, P. Champeil, J.V. Moller, *Biochim. Biophys. Acta – Biomembr.* 1508 (2000) 86.
- [13] A. Stenstam, G. Montalvo, I. Grillo, M. Gradzielski, *J. Phys. Chem. B* 107 (2003) 12331.
- [14] J.M. Lin, T.L. Lin, U.S. Jeng, Z.H. Huang, Y.S. Huang, *Soft Matter* 5 (2009) 3913.
- [15] E.L. Gelamo, R. Itri, A. Alonso, J.V. da Silva, M. Tabak, *J. Colloid Interface Sci.* 277 (2004) 471.
- [16] B. Schweitzer, D. Zanette, R. Itri, *J. Colloid Interface Sci.* 277 (2004) 285.
- [17] N. Gull, S. Chodankar, V.K. Aswal, P. Sen, R.H. Khan, *Colloids Surf. B – Biointerfaces* 69 (2009) 122.
- [18] S.K. Mehta, Bhawna, G. Ram, *J. Colloid Interface Sci.* 344 (2010) 105.
- [19] P.S. Goyal, S.V.G. Menon, B.A. Dasannacharya, P. Thiyagarajan, *Phys. Rev. E* 51 (1995) 2308.
- [20] J.A. Molina-Bolivar, J. Aguiar, C.C. Ruiz, *J. Phys. Chem. B* 106 (2002) 870.
- [21] P.S. Denkova, L. Van Lokeren, I. Verbruggen, R. Willem, *J. Phys. Chem. B* 112 (2008) 10935.
- [22] C.J. Drummond, G.G. Warr, F. Grieser, B.W. Ninham, D.F. Evans, *J. Phys. Chem.* 89 (1985) 2103.
- [23] G.L. Peterson, L.C. Rosenbaum, M.I. Schimerlik, *Biochem. J.* 255 (1988) 553.
- [24] A. delaMaza, J.L. Parra, *Biophys. J.* 72 (1997) 1668.
- [25] S.H. Lu, P. Somasundaran, *Langmuir* 23 (2007) 9188.
- [26] R. Smith, *Biochemistry* 21 (1982) 2697.
- [27] M. Le Maire, B. Arnou, C. Olesen, D. Georjgin, C. Ebel, J.V. Moller, *Nat. Protoc.* 3 (2008) 1782.
- [28] J. Lipfert, L. Columbus, V.B. Chu, S.A. Lesley, S. Doniach, *J. Phys. Chem. B* 111 (2007) 12427.
- [29] P. Timmins, E. Pebaypeyroula, W. Welte, *Biophys. Chem.* 53 (1994) 27.
- [30] N. Nelson, C.F. Yocum, *Annu. Rev. Plant Biol.* 57 (2006) 521.
- [31] B.S. Ko, B. Babcock, G.K. Jennings, S.G. Tilden, R.R. Peterson, D. Cliffl, E. Greenbaum, *Langmuir* 20 (2004) 4033.
- [32] J. Maly, J. Krejci, M. Ilie, L. Jakubka, J. Masojidek, R. Pilloton, K. Sameh, P. Steffan, Z. Stryhal, M. Sugiura, *Anal. Bioanal. Chem.* 381 (2005) 1558.
- [33] H.A. Kincaid, T. Niedringhaus, M. Ciobanu, D.E. Cliffl, G.K. Jennings, *Langmuir* 22 (2006) 8114.
- [34] M. Ciobanu, H.A. Kincaid, V. Lo, A.D. Dukes, G.K. Jennings, D.E. Cliffl, *J. Electroanal. Chem.* 599 (2007) 72.
- [35] I. Lee, J.W. Lee, E. Greenbaum, *Phys. Rev. Lett.* 79 (1997) 3294.
- [36] J.W. Lee, I. Lee, E. Greenbaum, *Biosens. Bioelectron.* 11 (1996) 375.
- [37] R.C. Williams, A.N. Glazer, D.J. Lundell, *Proc. Natl. Acad. Sci. USA – Biol. Sci.* 80 (1983) 5923.
- [38] X. Ruan, J. Wei, Q. Xu, J.-s. Wang, Y.-d. Gong, X.-f. Zhang, T.-y. Kuang, N.-m. Zhao, *J. Mol. Struct.* 525 (2000) 97.
- [39] F. Muh, A. Zouni, *Biochim. Biophys. Acta – Biomembr.* 1778 (2008) 2298.
- [40] J.F. Talling, D. Driver, in: M. Doty (Ed.), *Primary Productivity Measurements, Marine and Freshwater*, US Atomic Energy Commission, Washington, DC, 1963.
- [41] J. Happel, H. Brenner, *Low Reynolds Number Hydrodynamics with Special Applications to Particulate Media*, Martinus Hijhoff Publishers, The Hague, The Netherlands, 1983.
- [42] D. Mukherjee, M. Vaughn, B. Khomami, B.D. Bruce, *Colloids Surf. B: Biointer.*, submitted for publication.
- [43] J.G. Kirkwood, J.B. Shumaker, *Proc. Natl. Acad. Sci. USA* 38 (1952) 863.
- [44] A. Tardieu, A. Le Verge, M. Malfois, F. Bonnette, S. Finet, M. Ries-Kautt, L. Belloni, *J. Cryst. Growth* 196 (1999) 193.